https://doi.org/10.5194/egusphere-2023-2374
Preprint. Discussion started: 1 December 2023

Initial conditions control transport of volcanic volatiles, forcing and impacts

Zhihong Zhuo[1], Herman F. Fuglestvedt[1], Matthew Toohey[2], and Kirstin Krüger[1]

[1]Section for Meteorology and Oceanography, Department of Geosciences, University of Oslo, Oslo, Norway
[2]Institute for Space and Atmospheric Studies, University of Saskatchewan, Saskatoon, Canada

Correspondence: Zhihong Zhuo (zhihong.zhuo@geo.uio.no)

Abstract. Volcanic eruptions impact the climate and environment. The volcanic forcing is determined by eruption source parameters, including mass and composition of volcanic volatiles, eruption season, eruption latitude and injection altitude. Moreover, initial conditions of the climate system play an important role in shaping the volcanic response. However, our understanding of the combination of these factors, the distinctions between tropical and extratropical volcanic eruptions and the co–injection of sulfur and halogens remains limited. Here, we perform ensemble simulations of volcanic eruptions at 15° N and 64° N in January, injecting 17 Mt of SO_2 together with HCl and HBr at 24 km altitude, considering different initial conditions of the El Niño–Southern Oscillation, Quasi–Biennial Oscillation, and polar vortex. Our findings reveal that initial conditions control the transport of volcanic volatiles from the first month and modulate the subsequent latitudinal distribution of sulfate aerosols and halogens. This results in different volcanic forcing, surface temperature and ozone responses over the globe and Northern Hemisphere Extratropics (NHET) among the model ensemble members with different initial conditions. NH extratropical eruptions exhibit a larger NHET mean volcanic forcing, surface cooling and ozone depletion compared to tropical eruptions. However, tropical eruptions lead to more prolonged impacts compared to NH extratropical eruptions, both globally and in the NHET. The sensitivity of volcanic forcing to varying eruption source parameters and model dependency is discussed, emphasizing the need for future multi–model studies to consider the influence of initial conditions and eruption source parameters on volcanic forcing and subsequent impacts.

1 Introduction

Explosive volcanic eruptions can inject sulfur dioxide (SO_2), halogens, ash, and water vapor into the stratosphere, causing significant perturbation of the Earth system. Stratospheric sulfate aerosols formed from injected SO_2 reflect incoming solar radiation and absorb longwave radiation, cooling the surface and warming the stratosphere (Robock, 2000; Timmreck, 2012). A lot of studies have been conducted on the explosive eruption of Mt. Pinatubo in 1991 (Bluth et al., 1992; Guo et al., 2004; Robock, 2000; Ukhov et al., 2023). However, large uncertainties still exist in quantifying the amount of SO_2 injected into the stratosphere based on different observational (Bluth et al., 1992; Grant et al., 1992; Guo et al., 2004) and modelling (Dhomse et al., 2014; Jones et al., 2016; Mills et al., 2016; Niemeier et al., 2009; Quaglia et al., 2023; Stenchikov et al., 2021) studies. To reach the best agreement with Pinatubo volcanic forcing observations, models have used a wide range of SO_2 injections from 10

https://doi.org/10.5194/egusphere-2023-2374
Preprint. Discussion started: 1 December 2023

to 20 Tg (Timmreck et al., 2018). Atmosphere–aerosol models are mostly used, either with prescribed sea surface temperature (SST), such as MAECHAM5–HAM (Niemeier et al., 2009) and UM–UKCA (Dhomse et al., 2014), or in a fully coupled configuration with interactive atmosphere, ocean, sea–ice, chemistry and with a high model top, such as CESM–WACCM (Mills et al., 2016). Even when injecting the same SO_2 mass, models simulate different sulfate burden (Marshall et al., 2018) and stratospheric aerosol optical depth (SAOD) (Clyne et al., 2021; Zanchettin et al., 2016). Clyne et al. (2021) and Mills et al. (2017) argued that interactive OH chemistry is essential to accurately simulate the evolution and lifetime of volcanic aerosols. Quaglia et al. (2023) showed that with interactive aerosol microphysics, different stratospheric transport in different models is the main reason for their disagreement with Pinatubo observations.

Previous modelling studies on volcanic impacts mostly considered sulfur as the only volcanic volatile injection, ignoring the potential of volcanic halogens reaching the stratosphere (Krüger et al., 2015; Kutterolf et al., 2013, 2015; von Glasow et al., 2009; WMO, 2018). The few studies that simulated volcanic eruptions with co–injection of sulfur and halogens showed different volcanic forcing, ozone and climate responses compared to eruptions with sulfur–only injection (Brenna et al., 2019, 2020; Klobas et al., 2017; Lurton et al., 2018; Ming et al., 2020; Staunton-Sykes et al., 2021). However, these studies modelled different strengths of volcanic eruptions with different atmospheric background conditions. A more systematic model study investigating impacts of sulfur and halogen–rich tropical and extratropical eruptions is still lacking.

Different source parameters, including mass and composition of volcanic volatiles, eruption season, eruption latitude and eruption altitude, contribute to the source of large uncertainties that shape the forcing and impact of volcanic eruptions (Marshall et al., 2019; Metzner et al., 2014; Toohey et al., 2011, 2019; Zhuo et al., 2014, 2021). A key question lies in understanding how eruption latitude affects the forcing and impact of volcanic eruptions. Tropical eruptions were considered to have larger climate impact than extratropical eruptions (IPCC, 2013; Schneider et al., 2009). However, ice cores and tree ring reconstructions indicate that compared to historical tropical eruptions, extratropical eruptions led to larger climate impacts per unit volcanic stratospheric sulfate injection over the Northern Hemisphere (NH), which was supported by analysis of MAECHAM5–HAM model simulations (Toohey et al., 2019). Nevertheless, the results of this study are limited with regard to the aerosol and climate response as the ocean and sea ice were prescribed, next to the missing interaction of atmospheric chemistry and QBO. Using the fully coupled model MPI–ESM, Zhuo et al. (2021) simulated stronger NHET surface cooling after NH extratropical volcanic eruptions compared to tropical eruptions. However, this study used prescribed SAOD as volcanic forcing, which does not explicitly simulate the chemical, microphysical, and dynamical processes of the aerosols that play an important role in shaping the volcanic forcing and subsequent climate impact.

Post–eruption responses are affected by pre–eruption meteorological and climate initial conditions, including the initial states of the El Niño–Southern Oscillation (ENSO), Quasi–Biennial Oscillation (QBO) and polar vortex. The pre–eruption ENSO state modulates the post–eruption ENSO responses to volcanic eruptions and the surface winter warming pattern (Coupe and Robock, 2021; Khodri et al., 2017; Pausata et al., 2016, 2020). In the stratosphere, the QBO dominates the tropical circulation with alternating easterly and westerly winds, which plays an important role in the distribution of stratospheric aerosols and chemical constituents (Baldwin et al., 2001). Unlike ENSO and QBO, studies mostly considered the response of the polar vortex to tropical volcanic eruptions (Charlton-Perez et al., 2013; Toohey et al., 2014), but rarely considered how the initial

https://doi.org/10.5194/egusphere-2023-2374
Preprint. Discussion started: 1 December 2023

state of the polar vortex affects the volcanic forcing by influencing the distribution and evolution of aerosols from volcanic eruptions. In particular, differences in the impact of initial conditions on volcanic forcing and subsequent impacts between tropical and extratropical eruptions are unknown.

Here, we use a fully coupled Earth system model with interactive atmosphere, ocean, sea ice, and prognostic aerosol microphysics and atmospheric chemistry to simulate Pinatubo–magnitude eruptions at 15° N and 64° N in a pre–industrial atmosphere. We are particularly interested in how eruptions of this strength are affected by a QBO westerly phase, given the QBO disruption and prolonged easterly regime response to a tropical super eruption as modelled by Brenna et al. (2021). In addition, we apply different initial conditions of ENSO and polar vortex for our tropical and NH extratropical eruptions with sulfur and halogen injections. We also conduct sensitivity tests with sulfur injections only and in eruption season of July. In a related study by Fuglestvedt et al. (2023), we analyze the effects of initial polar vortex conditions on the aerosol evolution, volcanic forcing and deposition of NH extratropical eruption at 64° N. Here in this study, we aim to understand the following questions: What impacts do initial conditions have on transport of volcanic volatiles and volcanic forcing after tropical eruptions co–injecting sulfur and halogens? What differences do tropical and NH extratropical volcanic eruptions have on volcanic forcing and subsequent climate and ozone impacts?

In the following, we describe the data and methods in Sect. 2, including the model description and experimental design. In Sect. 3, we present the results. Sect. 3.1 shows the transport of SO_2 and aerosol controlled by initial conditions, which determines the volcanic forcing after tropical eruptions co–injecting sulfur and halogens. In Sect. 3.2, we compare the aerosol evolution, volcanic forcing, climate and ozone impact of tropical and NH extratropical eruptions under different initial conditions. The results are discussed in Sect. 4. Finally, we give the summary and conclusions in Sect. 5.

2 Data and Methods

2.1 Model description

This study uses the Community Earth System Model, version 2 (CESM2; Danabasoglu et al., 2020) with the high–top version of the atmosphere the Whole Atmosphere Community Climate Model, version 6 (WACCM6; Gettelman et al., 2019). WACCM6 has a horizontal resolution of 0.95° latitude by 1.25° longitude, with 70 hybrid sigma–pressure levels extending from the Earth's surface to 6×10^{-6} hPa (~140 km altitude). The ocean component, Parallel Ocean Program version 2 (POP2; Smith et al., 2010) runs at a nominal 1° horizontal resolution, with 60 vertical layers to 5,500 meters in depth. The same grid is used by the Los Alamos National Laboratory sea ice model, version 5 (CICE5; Hunke et al., 2015). The land component is the Community Land Model Version 5 (CLM5; Lawrence et al., 2019), with the Community Ice Sheet Model Version 2.1 (CISM2.1; Lipscomb et al., 2019) as its land–ice component.

WACCM6 uses a comprehensive chemistry configuration for the troposphere, stratosphere, mesosphere and lower thermosphere (TSMLT). It includes 231 solution species and 583 chemical reactions with 150 photolytic, gas–phase and heterogeneous reactions relevant for the whole atmosphere (Gettelman et al., 2019). The chemical families include O_x, HO_x, NO_x, ClO_x, BrO_x and SO_x. Aerosols are treated using the modified Modal Aerosol Model version 4 (MAM4; Liu et al., 2016) which

https://doi.org/10.5194/egusphere-2023-2374
Preprint. Discussion started: 1 December 2023

is coupled to cloud microphysics (Liu et al., 2012) and incorporates prognostic stratospheric aerosols (Mills et al., 2016). Validation of SO_2 emission and radiative forcing of volcanic eruptions confirms the qualification of the model for simulating volcanic eruptions and stratospheric aerosol geoengineering (Mills et al., 2016, 2017). WACCM6 also includes an internally generated QBO (Gettelman et al., 2019).

For model intercomparison, we also adopt MAECHAM5–HAM (Stier et al., 2005) for sensitivity tests. MAECHAM5–HAM is an aerosol–climate model with a T42 spectral truncation at ~2.8° × 2.8° spatial resolution and 39 vertical levels up to 0.01 hPa (~80 km). The model was run with free atmosphere and prescribed SSTs. Aerosol processes in the stratosphere are calculated by the aerosol microphysical module HAM (Niemeier et al., 2009; Toohey et al., 2011), which includes aerosol formation and growth via nucleation, condensation, accumulation and coagulation, sedimentation and final removal processes of wet and dry deposition. HAM uses a prescribed monthly mean OH field. This may affect the conversion of SO_2 to SO_4, which is dependent on the local consumption of OH. In addition, we also use the modular volcanic forcing generator EVA (Easy Volcanic Aerosol, Toohey et al., 2016). It prescribes the SAOD and serves as the tool for compiling the volcanic forcing for experiments in the Paleoclimate Model Intercomparison Project 4 (Jungclaus et al., 2017; Sigl et al., 2015, 2022; Toohey and Sigl, 2017).

2.2 Experimental design

A spin–up run for 56 years is conducted under pre–industrial 1850s conditions, from which we pick six initial conditions considering different El Niño–Southern Oscillation (ENSO), and polar vortex (PV) states with westerly Quasi–Biennial Oscillation (QBO) (see Section 2.3) to conduct ensemble runs (Table 1). These baseline ensemble experiments include both volcanic sulfur and halogen injections. Tropical eruptions are located at 15° N, 91° W (H–15N–Jan), simulating Central American Volcanic Arc (CAVA) eruptions, while NH extratropical eruptions are located at 64° N, 19° W (H–64N–Jan), simulating eruptions of the Katla volcanic system over Iceland. We use January as the base eruption season, as this is the default for historical volcanic eruptions when the eruption season is unknown in ice–core–based volcanic forcing reconstructions (Sigl et al., 2022; Toohey and Sigl, 2017). Following Toohey et al. (2019), we inject 17 Tg SO_2 at 24 km altitude, mimicking a Pinatubo–like eruption, but in a pre–industrial 1850s atmosphere taking the co–injection of sulfur and halogens into account. The injected HCl and HBr masses are based on estimation of CAVA eruptions (Kutterolf et al., 2013, 2015), assuming a conservative injection efficiency of 10% for tropical eruptions to the stratosphere (Brenna et al., 2019; Krüger et al., 2015) but applied here for both eruption latitudes for comparability. Except for the baseline experiments, we also run simulations injecting only SO_2 at 15° N (S–15N–Jan) and 64° N (S–64N–Jan), to test the difference between volcanic eruptions with co–injection of sulfur and halogens and sulfur–only injection. We run a set of eruptions in July at 15° N (H–15N–Jul and S–15N–Jul) and 64° N (H–64N–Jul and S–64N–Jul), to test the impact of eruption season on the volcanic forcing and related impacts. A control run lasts for 30 years without volcanic injection is conducted.

For comparison, we use model data from Toohey et al. (2019) simulating volcanic eruptions with 17 Tg SO_2 injection at 15° N in both January and July with MAECHAM5–HAM (ECHAM5–15N–Jan/Jul). For tropical eruptions, we calculate ensemble member mean with five members each. For NH extratropical eruptions at 64° N, two additional runs from

https://doi.org/10.5194/egusphere-2023-2374
Preprint. Discussion started: 1 December 2023

ECHAM5–64N–Jan/Jul are available for comparison (this study). We also calculated the volcanic forcing from EVA (EVA–15N–Jan/Jul and EVA–64N–Jan/Jul).

The set of experiments is summarized in Table 1.

2.3 Analysis methods

We adopt the Oceanic Niño Index (ONI; https://www.climate.gov/news-features/understanding-climate/climate-variability-oceanic-nino-index) to quantify the initial ENSO state. The ONI is calculated from a three–month running mean of the average sea surface temperature (SST) anomalies over the Niño 3.4 region covering 5° N–5° S and 170° W–120° W. The SST anomalies are calculated with respect to the 30–year mean of the control run without volcanic eruption. The QBO is calculated with the monthly equatorial mean zonal wind at 30 hPa between 2° N–2° S.

We present both the ensemble members and the ensemble means of adopted variables to study the volcanic forcing and subsequent impacts. Anomalies are calculated with respect to the 30–year mean of the control run. The ensemble standard deviation is calculated to indicate the spread of the baseline ensemble experiments.

3 Results

3.1 Initial conditions control aerosol transport and volcanic forcing after tropical eruptions

Tropical eruptions have usually been thought to have a larger climate impact than extratropical eruptions, as SO_2 and formed aerosols are transported to both the Northern and Southern Hemispheres. Here, we examine how initial conditions affect the transport and evolution of volcanic volatiles and subsequent volcanic forcing after tropical eruptions.

Figure 1a shows the first month latitudinal distribution of SO_2 after the 15° N tropical eruptions in January, which diverges among the baseline ensemble experiments. We have ordered the baseline experiments H1 to H6 according to less to more northward transport of volcanic volatiles, respectively. Note that this labeling differs from Fuglestvedt et al. (2023), who ordered their ensemble members based on the stability of the polar vortex. During this boreal winter season, wave breaking is stronger in the winter hemisphere leading to strong mixing and distribution toward the NH high latitudes, which is evident especially in H6. In contrast, when SO_2 is distributed more equatorward, less SO_2 is distributed to the NH, as shown especially in H1. The latitudinal distribution of SO_2 in the first month modulates the subsequent latitudinal distribution of SO_4. Figure 1b shows the latitudinal distribution of the sixth month SO_4 column burden for the six ensemble members. More SO_4 is transported to the NH high latitudes between 30° N and 90° N in H6 compared to the other members, especially in H1 and H2. Differences in the transport of SO_2 and SO_4 result in differences in cumulative volcanic forcing in the NH and SH high latitudes among the ensemble members (Fig. 1c). H6 shows a strong asymmetric volcanic forcing with large meridional forcing differences, i.e., cumulative SAOD up to 8.4 between the NH and the SH, while H1 shows relatively symmetric volcanic forcing between the hemispheres. Here, even with the same eruption source parameters, volcanic eruptions in the tropics result in different symmetries of the volcanic forcing only due to different initial conditions. For tropical eruptions, the initial conditions control

https://doi.org/10.5194/egusphere-2023-2374
Preprint. Discussion started: 1 December 2023

the transport of SO_2 from the first month, to the formation and transport of SO_4 in the coming months and determine the latitudinal distribution of the sulfate aerosol and subsequent volcanic forcing.

Figure 1d shows the latitudinal and vertical distribution of SO_2 and residual vertical velocity of the first post–eruption month for the six ensemble members. The SO_2 reaches higher altitudes but relatively less towards the NH extratropics in members H1 to H6. Notably, in H5 and H6, with greater transport of SO_2 to NH mid–latitudes, there is comparatively lower upward transport of SO_2 compared to the other members. Consequently, this leads to accelerated formation and transport of sulfate aerosol towards the NH high latitudes in the following months (Fig. 1b). The residual vertical velocity (w*, contour in Fig. 1d) reveals the upward mass transport in the tropics and the subsequent downward transport in the extratropics of the winter hemisphere in January. This reflects the large–scale Brewer–Dobson circulation in the stratosphere (Butchart, 2014). Tropical injections at 15° N are within the ascending branch of the BD circulation but near the surf zone in the extratropics. A stronger upward transport in the tropics is evident when the volcanic SO_2 injection is further away from the zero line of w*, as shown in H1 and H2 in comparison to H5 and H6.

The initial conditions control not only the SO_2 and sulfate aerosol transport but also the volcanic halogen transport. More total chlorine and total bromine are transported to NH high latitudes in H6 compared to H2 and H1 (see Section 3.2.3).

The control of initial conditions on aerosol and halogen transport and subsequent volcanic forcing is not only evident for tropical eruptions but also for NH extratropical eruptions, although with a different dominating factor. For NH extratropical eruptions at 64° N in January, the initial polar vortex conditions play a dominant role in the transport and evolution of SO_2 as further investigated in our related paper by Fuglestvedt et al. (2023).

3.2 Comparison of tropical and NH extratropical volcanic eruptions with sulfur and halogens injection

3.2.1 SO_2 and aerosol evolution determines volcanic forcing

Figure 2 shows time series of global and NHET SO_2, SO_4, aerosol effective radius (R_{eff}) and stratospheric aerosol optical depth (SAOD). The global SO_2 burden reduces faster in the first months after tropical eruptions (H–15N–Jan, solid lines) compared to NH extratropical eruptions (H–64N–Jan, dashed lines) with an average e–folding time of 2.6 months and 3 months, respectively (Fig. 2a). Along with the reduction of SO_2, SO_4 forms within the first post–eruption month. The maximum global SO_4 burden after tropical and NH extratropical eruptions is almost the same, reaching up to 30 Tg, 9 months after the tropical eruptions but 5 months after the NH extratropical eruptions (Fig. 2c). Differences in the transport of SO_2 lead to different peak timing of SO_4 after tropical and NH extratropical eruptions. As is reflected by the NHET SO_2 burden (Fig. 2b), after tropical eruptions (solid lines), SO_2 increases in the first 1 to 2 months and then decreases and disappears 4 to 5 months after the eruption, while showing a gradual transport of SO_2 from the tropics to NH high latitudes. Meanwhile, the NHET SO_4 burden exhibits a sharp increase in the first 4 to 5 months, followed by a decelerated increase, ultimately peaking around 12 months after the tropical eruptions (Fig. 2d). After the NH extratropical eruptions (dashed lines), due to confinement of the aerosols in the NHET region, global and NHET SO_2 and SO_4 burden show similar evolution (Fig. 2a–2d). The duration of global SO_4

https://doi.org/10.5194/egusphere-2023-2374
Preprint. Discussion started: 1 December 2023

burden is affected by the transport of SO_2 from tropical to NH extratropical regions, which is longer for tropical eruptions over 54 months in contrast to NH extratropical eruptions over 36 months.

As shown in Figure 1, the initial conditions control the transport of volcanic volatiles. The poleward transport of SO_2 and evolution of SO_4 in the NHET (Fig. 2b and 2d) show a large spread among the six ensemble members of tropical eruptions. More SO_2 is transported to NHET in H6 than in H1, leading to a higher peak NHET SO_4 burden in H6 than in H1. Meanwhile, the global SO_4 burden shows a faster reduction from its maximum in H6 than in H1 (Fig. 2c). In general, increased NHET transport after tropical eruptions is accompanied by a faster reduction of global SO_4 burden (Fig. 2c).

The aerosol size grows through condensation and coagulation along the conversion of SO_2 to SO_4 in the stratosphere. In line with the conversion of SO_2 to SO_4, the global–mean SO_4–mass–weighted mean effective radius (R_{eff} , Fig. 2e) increases faster after tropical eruptions compared to NH extratropical eruptions for the first 6 months. R_{eff} further increases 7–9 months after tropical eruptions when the peak has already been reached after NH extratropical eruptions, and it decreases slower after tropical eruptions compared to NH extratropical eruptions. This is similar for the NHET–mean R_{eff} (Fig. 2f) with a smaller but later peak after tropical eruptions compared to NH extratropical eruptions. This agrees with the varied lifetime of SO_2 and SO_4 burden (Fig. 2a–2d). For tropical eruptions, it takes time for SO_2 to be transported northward, and the amount of SO_2 transported to the NHET region varies due to different initial conditions (Fig. 2b). This is also reflected by different R_{eff} in different ensemble members. After tropical eruptions, the NHET–mean R_{eff} is larger in maximum, i.e., 0.43 μm in H6 compared to 0.38 and 0.39 μm in H1 and H2, and decreases faster in H6 than in H1 and H2 (Fig. 2f), indicating a faster removal of larger aerosols with larger gravitational settling velocity than for small aerosols. In line with this, less SO_4 is available outside of NHET regions. Thus, the maximum global–mean R_{eff} is 0.31 μm in H6, smaller than 0.36 μm in H1 and 0.37 μm in H2 (Fig. 2e). For NH extratropical eruptions, the aerosol size grows continuously with SO_2 concentrated in the NHET region.

SO_2, SO_4, R_{eff} and SAOD evolution are tightly connected and modulated by initial conditions. The volcanic forcing is primarily determined by the SO_4 burden when the aerosol size exceeds the peak scattering efficiency at 0.25 μm (Lacis, 2015), as shown by a consistent evolution of the global–mean and NHET–mean SAOD (Fig. 2g and 2h). The maximum global–mean SAOD shows a similar magnitude (~0.2) after tropical and NH extratropical eruptions, but it takes longer to reach the maximum and the forcing lasts longer after tropical eruptions compared to NH extratropical eruptions. Due to the wider spread of aerosols, tropical eruptions result in a smaller and delayed peak of NHET–mean SAOD, but a longer–lasting forcing compared to NH extratropical eruptions, after which aerosols are confined in the NHET region.

3.2.2 Climate impact

Figure 3 shows the surface temperature response in the ensembles of tropical and NH extratropical eruptions. Both global–mean (Fig. 3a and 3c) and NHET–mean surface temperature (Fig. 3b and 3d) show a weaker but longer–lasting surface cooling after tropical eruptions (Fig. 3a and 3b) compared to NH extratropical eruptions (Fig. 3c and 3d). The strongest surface cooling emerges in the second and first year after tropical and NH extratropical eruptions, respectively.

https://doi.org/10.5194/egusphere-2023-2374
Preprint. Discussion started: 1 December 2023

The season when the volcano erupts plays an important role in the temperature variation. When volcanoes erupt in January, both global–mean and NHET–mean SAOD peak around 12 months after tropical eruptions (Fig. 2g and 2h). During boreal winter, less incoming solar radiation reaches the NH. This interrupts the reduction of net radiation at the top of the atmosphere (TOA) (Fig. S1a and S1b) and surface temperature, thus, the cooling peaks in the second year after tropical eruptions (Fig. 3a and 3b). Both global–mean and NHET–mean SAOD peak 5 months after NH extratropical eruptions (Fig. 2g and 2h). This occurs during the boreal summer when the NH experiences its highest solar radiation influx. This synchronization between largest volcanic forcing and largest incoming solar radiation leads to the largest reflection of solar radiation (not shown) and subsequent decrease of TOA net radiation (Fig. S1c and S1d), thus result in the strongest surface cooling in the first year (Fig. 3c and 3d).

The surface cooling persists longer after tropical eruptions than NH extratropical eruptions, with variations among the members. Different surface temperature responses in different ensemble members are related to the transport of volcanic volatiles under different initial conditions. This is pronounced in the NHET–mean surface temperature responses after tropical eruptions (Fig. 3b). The NHET surface cooling is stronger 5 to 12 months after the eruption in H6 compared to H1, reflecting the distribution of SO_4 into the NH (Fig. 2d). In addition, the initial ENSO state impacts the temperature response, as reflected by positive global–mean surface temperature anomalies in the first two post–eruption months in H1 and H2 (Fig. 3a and 3c) under initial El Niño states (Table 1) for both tropical and extratropical eruptions.

3.2.3 Halogen–ozone impact

Figure 4 shows the evolution of total inorganic halogen burden and the ozone response. Injected HCl and HBr in the stratosphere reacts with OH to produce chlorine and bromine radicals, reacting with ozone in a catalytic destruction cycle (Solomon, 1999). The global total inorganic chlorine burden shows an e–folding time of 48 and 18 months after tropical and NH extratropical eruptions, including a sizeable plateau at the beginning (Cl_y, Fig. 4a). Global total inorganic bromine burden (Br_y, Fig. 4c) increases for approximately 14 and 6 months after tropical and NH extratropical eruptions, then decreases with e–folding times of 54 and 22 months, respectively. NHET Cl_y and Br_y burdens (solid lines in Fig. 4b and 4d) increase for approximately 14 months, then followed by a continuous decrease with a slight seasonal variation, indicating the transport of halogens into the NHET after tropical eruptions. Halogens are concentrated in the NHET after NH extratropical eruptions, as NHET Cl_y and Br_y burdens (dashed lines in Fig. 4b and 4d) decrease immediately and continuously except for slight variations during the first months. Different ensemble members of tropical eruptions show large differences in the magnitude of NHET Cl_y and Br_y burden, with a larger peak in H6 than in H1 and H2. This indicates that the control of initial conditions on SO_2 and aerosol transport is also representative for halogen transport. The longer transport time to NH high latitudes after tropical eruptions also contributes to a longer lifetime of both global and NHET Cl_y and Br_y burden, compared to NH extratropical eruptions (Fig. 4a–4d).

In response to the eruptions with co–injection of sulfur and halogens, global–mean and NHET–mean column ozone decreases (Fig. 4e and 4f). Compared to NH extratropical eruptions, tropical eruptions lead to a similar maximum but a delayed peak and longer–lasting global–mean ozone depletion, which lasts over 5 years (Fig. 4e). Due to confinement of halogens

https://doi.org/10.5194/egusphere-2023-2374
Preprint. Discussion started: 1 December 2023

in the NHET region, NH extratropical eruptions lead to a stronger NHET–mean ozone depletion than tropical eruptions, but the ozone depletion lasts longer after tropical eruptions compared to NH extratropical eruptions. Notably, the NHET–mean column ozone drops below 220 DU, projecting NH ozone hole risks after both tropical and NH extratropical eruptions (Fig. 4f). A larger NHET halogen burden (Fig. 4b and 4d) leads to a stronger NHET–mean ozone depletion in H6 than in H1 and H2 after tropical eruptions. Enhanced northward transport of halogens leads to faster removal as well as less availability of halogens in the tropics and Southern Hemisphere. Thus, global–mean halogen burden decreases faster in H6 than in H1 and H2 (Fig. 4a–4d). This leads to earlier depletion and recovery of ozone over both the globe and NHET in H6 than in H1 and H2 (Fig. 4e and 4f).

4 Discussion

4.1 Control of initial conditions on the transport of volcanic volatiles

We interpret the control of the initial conditions on the transport of volcanic volatiles after tropical eruptions to be related to the secondary meridional circulation associated with the QBO (Baldwin et al., 2001) and the "leaky pipe" concept of stratospheric circulation in the tropics (Neu and Plumb, 1999). H1 and H2 reveal enhanced upward transport of SO_2, whereas H5 and H6 reveal less upward but more meridional transport towards NH high latitudes (Fig. 1). This stronger leak of SO_2 out of the tropical pipe (for H5 and H6 in contrast to H1 and H2) relates to a stronger stratospheric secondary meridional circulation under a more intense QBO westerly phase (Fig. S2) connected with a larger temperature contrast between tropical and NH mid–latitudes (Fig. S3). As pointed out by Ribera et al. (2004), during a strong QBO westerly phase, enhanced ascent of air in the stratosphere is associated with a cooling anomaly in the equatorial area between 15° S and 15° N, while an opposite warming anomaly in the mid–latitudes between 15° N and 55° N relates to an enhanced adiabatic sinking. This is reflected in our model results following tropical eruptions (Fig. 1d and S3).

The control of initial conditions on the transport of volcanic volatiles is also evident after NH extratropical eruptions, in this case primarily controlled by the initial polar vortex state. The northward transport and lifetime of SO_2 increases from members 1 to 6 (Fuglestvedt et al., 2023) with increasing initial polar vortex stability. Notably, the order of the ensemble members differs between tropical and NH extratropical eruptions, underlining different factors controlling the transport of volcanic volatiles following tropical and NH extratropical eruptions. However, in both this study and Fuglestvedt et al. (2023), the ensembles exhibit less northern poleward transport of SO_2 in the first to fourth members, as compared to the fifth and sixth members. The former four members (H1 to H4) correspond to El Niño or neutral ENSO initial states, while the latter two members (H5 and H6) correspond to La Niña states (Table 1). As highlighted in van Loon and Labitzke (1987), El Niño events are typically linked to a warming and weakening of the polar vortex, along with a cooling in the tropical lower stratosphere, however, unusual warming occurs when a simultaneous injection of volcanic gases and aerosols takes place. In contrast, La Niña events often demonstrate a strengthening of the polar vortex.

Overall, we interpret our results as being primarily influenced by initial conditions such as the state of the QBO, ENSO, and the stratospheric polar vortex. These factors collectively control the transport of volcanic volatiles and aerosols and ultimately

https://doi.org/10.5194/egusphere-2023-2374
Preprint. Discussion started: 1 December 2023

determine the volcanic forcing. Certainly, ambient meteorological conditions introduce an element of unpredictability to the dispersion of volcanic materials out of the tropics. However, as highlighted by Jones et al. (2016), this dispersion is particularly sensitive to ambient meteorological conditions for low–altitude eruptions (16–18 km). In contrast, a high–altitude eruption scenario (19–29 km) exhibits reduced meteorological variability, a phenomenon to which our simulations, with injection altitude of 24 km, appear to be less susceptible. Our results reveal the potential for predicting the latitudinal distribution of volcanic volatiles and assessing the subsequent volcanic forcing and associated climate and environmental impacts already after the first month of tropical and NH extratropical eruptions. Other models and ensemble members are necessary to validate these findings, and to test different initial states with the QBO easterly phase. Zanchettin et al. (2022) recommended improving the assessment of initial condition influences on direct radiative and dynamical responses. The future phase of the VolMIP holds potential as a valuable resource for addressing these research needs.

4.2 Comparisons between tropical and NH extratropical eruptions

Based on tree ring proxy data and MAECHAM5–HAM model simulations, Toohey et al. (2019) concluded that compared to NH extratropical eruptions, tropical eruptions lead to weaker maximum volcanic forcing over the NHET for a given injection height with sulfur–only injection. Figure 5 presents an overall summary of the comparison between tropical and NH extratropical eruptions regarding their maximum volcanic forcing and impacts on surface temperature and ozone. Our fully coupled model results confirm the results from Toohey et al. (2019), also when co–injecting sulfur and halogens and resolving interactive atmospheric chemistry for the simulated volcanic eruptions. However, when considering the time–to–maximum and the lifetime, tropical eruptions cause longer–lasting volcanic forcing and surface cooling compared to NH extratropical eruptions, over both the globe and NHET. The delayed response time after tropical eruptions results from the northward transport of stratospheric aerosols (Fig. 2). Sulfur was the only injected volcanic volatile and OH was prescribed in MAECHAM5–HAM. Thus, the timing difference is lacking for eruptions at different latitudes in Toohey et al. (2019). Including interactive atmospheric chemistry and OH in models can be important in order to simulate the timing of volcanic aerosol evolution, volcanic forcing and subsequent impact, as previously also noted by Mills et al. (2017) and Clyne et al. (2021).

4.3 Sensitivity to varying eruption source parameters

Here we discuss how sensitive our results are to varying eruption source parameters. Figure 6 shows the global–mean and NHET–mean SAOD, surface temperature and column ozone variations after tropical and NH extratropical eruptions with different volcanic volatile injections and in different seasons. We focus on testing sulfur–only injections and eruptions in July (see Table 1). The maximum global–mean SAOD is larger in H–15N–Jan than in S–15N–Jan, and even larger in H–15N–Jul than in S–15N–Jul. Besides, both S–15N–Jan and S–15N–Jul fall outside the H–15N–Jan $\pm 2\sigma$ range (Fig. 6a). This result seems to be consistent with the study using the UKESM by Staunton-Sykes et al. (2021), who modelled a larger global–mean SAOD after tropical eruptions in July with co–injection of sulfur and halogens than sulfur–only injection. However, this relationship is also dependent on the eruption latitude. After NH extratropical eruptions, the difference of global–mean SAOD is limited and differs after eruptions in different seasons (Fig. 6c). The maximum NHET–mean SAOD (Fig. 6b and 6d) and surface

https://doi.org/10.5194/egusphere-2023-2374
Preprint. Discussion started: 1 December 2023

temperature response (Fig. 6e–6h) also varies among different experiments with varying volcanic volatiles as well as eruption latitudes and eruption seasons. Nonetheless, these responses are mostly within the range of H–15N–Jan $\pm 2\sigma$ and H–64N–Jan $\pm 2\sigma$, indicating a potential larger impact of varying initial conditions than tested varying eruption source parameters on the volcanic forcing and subsequent surface cooling.

Varying volcanic volatiles, particularly with or without halogen injection, has a significant impact on stratospheric ozone under pre–industrial conditions. In line with Brenna et al. (2020), volcanic eruptions with co–injection of sulfur and halogens result in substantial ozone depletion (solid lines), while volcanic eruptions with sulfur–only injection (dashed lines) slightly increase global and NHET ozone levels (Fig. 6i and 6j). Co–injection of sulfur and halogens leads to similar maximum ozone depletion after tropical and NH extratropical eruptions in January (H–15N–Jan and H–64N–Jan), but a stronger ozone depletion occurs after the tropical eruption compared to the NH extratropical eruption in July (H–15N–Jul and H–64N–Jul). For eruptions at the same latitude, the maximum ozone loss is larger in H–15N–Jul than in H–15N–Jan, but smaller in H–64N–Jul than in H–64N–Jan. The increase of ozone following sulfur–only injections is stronger after tropical eruptions compared to NH extratropical eruptions. Tropical sulfur–only eruptions lead to significant ozone increases (S–15N–Jan and S–15N–Jul), while ozone responses after NH extratropical eruptions (S–64N–Jan and S–64N–Jul) mostly fall within the range of two standard deviations of the control run. The impact of tested varying source parameters is generally smaller than the impact of varying initial conditions, as the sensitivity experiments mostly fall within the modelled range of H–15N–Jan $\pm 2\sigma$ and H–64N–Jan $\pm 2\sigma$. Further studies with ensembles for the sensitivity tests are needed to further clarify the role of initial conditions and varying eruption source parameters in affecting volcanic forcing and subsequent climate and environmental impacts.

In this study, we only considered the co–injection of sulfur and halogens. Zhu et al. (2020) and Stenchikov et al. (2021) have shown that co–injection of sulfur, ash and water vapor affect the composition, distribution and radiative forcing of a volcanic cloud during the first months. However, whether these volcanic materials influence the maximum, time–to–maximum and lifetime of volcanic forcing in combination with sulfur and halogen injections has not been studied yet. Future simulations that incorporate these volcanic materials are needed to investigate how they affect the results shown in this study.

4.4 Model dependency

Clyne et al. (2021), Marshall et al. (2018) and Quaglia et al. (2023) showed that the impacts of varying source parameters on volcanic forcing and related climate responses are model dependent. Here, we discuss our model results on sulfur–only injection experiments with MAECHAM5–HAM and EVA (Fig. 6). After tropical eruptions, similar maximum global–mean SAOD emerges after January and July eruptions in MAECHAM5–HAM (green lines), but peaks at least 6 months earlier than in CESM2–WACCM6 (red dashed lines, Fig. 6a). This may relate to the interactive OH in CESM2–WACCM6 (Fig. S4). Maximum NHET–mean SAOD in MAECHAM5–HAM is smaller compared to CESM2–WACCM6 (Fig. 6b). For NH extratropical eruptions, maximum global and NHET–mean SAOD is much smaller after July eruption compared to January eruption in MAECHAM5–HAM, but limited differences are shown in CESM2–WACCM6 (Fig. 6c and 6d). In comparison, EVA (gray lines) generally produces smaller SAOD compared to CESM2–WACCM6 and MAECHAM5–HAM, except for that in MAECHAM5–HAM–64N–Jul (Fig. 6b). The inter–model difference shown in this study agrees with Clyne et al. (2021),

https://doi.org/10.5194/egusphere-2023-2374
Preprint. Discussion started: 1 December 2023

where CESM–WACCM showed the largest maximum global–mean, the longest time–to–maximum, and the longest duration of the SAOD. Notably, CESM–WACCM produced the smallest global mean stratospheric effective radius among the models. For Pinatubo–strength simulations, our CESM2–WACCM6 results also indicate a smaller global–mean R_{eff} ($\tilde{0}.35$ μm) compared to a R_{eff} exceeding 0.4 μm with MAECHAM5–HAM (Toohey et al., 2019)). These differences can arise from different model top, aerosol microphysics or chemistry resolved in model configurations. Zanchettin et al. (2022) showed that, under the VolMIP protocol, the maximum global–mean surface cooling ranges between 0.27 °C and 0.38 °C in ensemble means of six models simulating the Pinatubo eruption, which is lower than the analyzed 0.5 °C cooling based on HadCRUT5 observational data. In comparison, our CESM2–WACCM6 runs simulate a global–mean maximum cooling up to 0.6 °C in S–15N–Jul. In line with Zanchettin et al. (2016), CESM2–WACCM6 represents an upper threshold among the models.

5 Summary and conclusions

In this study, we perform idealized experiments with CESM2–WACCM6 to compare tropical and Northern Hemisphere extratropical volcanic eruptions in terms of the evolution of volcanic volatiles and aerosols, volcanic forcing and subsequent impacts on surface temperature and ozone. We consider in particular the co–injection of sulfur and halogens to the stratosphere under pre–industrial 1850s conditions and investigate the sensitivity to initial conditions. We ran two sets of baseline experiments with volcanic eruptions in January at 15° N and 64° N co–injecting SO_2 and halogens (HCl, HBr) into the stratosphere at 24 km altitude. Each set has six ensemble members with westerly QBO and varying ENSO and polar vortex initial states. We also performed sensitivity tests varying volcanic volatiles (sulfur only) and eruption season (July).

Our model results reveal that initial conditions control the meridional transport of sulfur and halogens in the first month after the eruptions, and further modulate the latitudinal distribution of sulfate aerosols, halogens, volcanic forcing and impacts. The baseline experiments, with the same eruption source parameters but different initial conditions, show large variations in the volcanic forcing and subsequent climate and ozone impacts. For tropical eruptions, the initial conditions also control the hemispheric asymmetry of the volcanic forcing.

Tropical and NH extratropical volcanic eruptions co–injecting SO_2 and halogens lead to similar maximum global–mean aerosol forcing, surface cooling and ozone depletion. However, for NHET–mean responses, the NH extratropical eruptions have a larger maximum impact than tropical eruptions. For both global–mean and NHET–mean volcanic forcing, climate and ozone impacts, tropical eruptions take longer to peak and last longer than NH extratropical eruptions. Thus, when evaluating whether tropical or NH extratropical eruptions have larger climate and environmental impacts, it is important to evaluate both the severity and the duration of the impact, as different perspectives can come to different conclusions.

Compared to volcanic eruptions with sulfur–only injection, co–injection of sulfur and halogens leads to large differences in the ozone responses. Under pre–industrial conditions, volcanic eruptions with sulfur–only injections lead to a slight increase of ozone. In contrast, co–injection of sulfur and halogens leads to a significant ozone depletion lasting more than 5 years after tropical eruptions and up to 5 years after NH extratropical eruptions of Pinatubo–strength.

https://doi.org/10.5194/egusphere-2023-2374
Preprint. Discussion started: 1 December 2023

Compared to varying source parameters of volcanic eruptions, varying initial conditions reveal an important impact on the volcanic forcing and subsequent climate and ozone impacts. The impact has a larger variability at the early stage after tropical eruptions than after NH extratropical eruptions, as initial conditions lead to large differences in the transport of volcanic volatiles and aerosols from tropics to high latitudes already from the first post-eruption month. For NH extratropical eruptions, the variability of surface temperature response increases over time, especially during winter.

Both CESM2–WACCM6 and MAECHAM5–HAM model results show varied global–mean and NHET–mean SAOD with eruptions at different latitudes and in different seasons. Compared to both models, EVA produces similar forcing duration but smaller global–mean and NHET–mean maximum SAOD, and with limited variations to different eruption latitudes and eruption seasons. The differences in volcanic forcing revealed here underscores potential large discrepancy between utilizing Earth system models with interactive atmospheric chemistry and models with prescribed SAOD generated with EVA to examine the influence of varying initial conditions and source parameters on volcanic forcing and subsequent impacts.

Initial conditions and eruption source parameters seem to be key for understanding the difference and comparability between simulations and observations of forcing and impacts of volcanic eruptions. Our study highlights the large variability of volcanic forcing and response with varying initial conditions, which is comparable to that with varying eruption source parameters. Multi–model simulations and comparisons are needed to further test our results. Our results point to the necessity of including initial conditions in future VolMIP protocols for better understanding volcanic impacts on the climate and environment.

Data availability. The CESM2–WACCM6 data generated and analysed for the current study are available in the NIRD Research Data Archive.

Author contributions. Z.Z. analysed data, wrote the manuscript, and led the discussion with input from all authors. Z.Z., K.K. and H.F. designed the CESM2–WACCM6 experiments, and Z.Z. and H.F. conducted the CESM2–WACCM6 simulations. M.T. and K.K. designed the MAECHAM5–HAM experiments, and M.T. conducted the simulations. K.K. initiated and led the research project.

Competing interests. One of the (co-)authors is a member of the editorial board of Atmospheric Chemistry and Physics.

Acknowledgements. This work is funded by the Norges Forskningsråd/University of Oslo Toppforsk project “VIKINGS” with grant number 275191. We acknowledge the Norwegian Research Infrastructure Services (NRIS)–Sigma2 for providing computer resources for model simulations on Fram cluster and data storage and data processing on NIRD cluster. The MAECHAM5–HAM simulations were performed at the Germany Climate Computer Center (Deutsch Klimazentrum, DKRZ) and funded by the Federal Ministry for Education and Research in Germany (BMBF) through the research program “MiKlip” (grant nos FKZ: 01LP130B, 01LP1130A and 01LP1517B).

https://doi.org/10.5194/egusphere-2023-2374
Preprint. Discussion started: 1 December 2023

References

Baldwin, M. P., Gray, L. J., Dunkerton, T. J., Hamilton, K., Haynes, P. H., Randel, W. J., Holton, J. R., Alexander, M. J., Hirota, I., Horinouchi, T., Jones, D. B. A., Kinnersley, J. S., Marquardt, C., Sato, K., and Takahashi, M.: The quasi-biennial oscillation, Rev. Geophys., 39, 179–229, https://doi.org/https://doi.org/10.1029/1999RG000073, 2001.

Bluth, G. J. S., Doiron, S. D., Schnetzler, C. C., Krueger, A. J., and Walter, L. S.: Global tracking of the SO2 clouds from the June, 1991 Mount Pinatubo eruptions, Geophys. Res. Lett., 19, 151–154, https://doi.org/https://doi.org/10.1029/91GL02792, 1992.

Brenna, H., Kutterolf, S., and Kruger, K.: Global ozone depletion and increase of UV radiation caused by pre-industrial tropical volcanic eruptions, Sci. Rep., 9, 9435, https://doi.org/10.1038/s41598-019-45630-0, 2019.

Brenna, H., Kutterolf, S., Mills, M. J., and Krüger, K.: The potential impacts of a sulfur- and halogen-rich supereruption such as Los Chocoyos on the atmosphere and climate, Atmos. Chem. Phys., 20, 6521–6539, https://doi.org/10.5194/acp-20-6521-2020, 2020.

Brenna, H., Kutterolf, S., Mills, M. J., Niemeier, U., Timmreck, C., and Krüger, K.: Decadal Disruption of the QBO by Tropical Volcanic Supereruptions, Geophys. Res. Lett., 48, https://doi.org/10.1029/2020gl089687, 2021.

Butchart, N.: The Brewer-Dobson circulation, Rev. Geophys., 52, 157–184, https://doi.org/10.1002/2013rg000448, 2014.

Charlton-Perez, A. J., Baldwin, M. P., Birner, T., Black, R. X., Butler, A. H., Calvo, N., Davis, N. A., Gerber, E. P., Gillett, N., Hardiman, S., Kim, J., Krüger, K., Lee, Y.-Y., Manzini, E., McDaniel, B. A., Polvani, L., Reichler, T., Shaw, T. A., Sigmond, M., Son, S.-W., Toohey, M., Wilcox, L., Yoden, S., Christiansen, B., Lott, F., Shindell, D., Yukimoto, S., and Watanabe, S.: On the lack of stratospheric dynamical variability in low-top versions of the CMIP5 models, J. Geophys. Res. Atmos., 118, 2494–2505, https://doi.org/10.1002/jgrd.50125, 2013.

Clyne, M., Lamarque, J.-F., Mills, M. J., Khodri, M., Ball, W., Bekki, S., Dhomse, S. S., Lebas, N., Mann, G., Marshall, L., Niemeier, U., Poulain, V., Robock, A., Rozanov, E., Schmidt, A., Stenke, A., Sukhodolov, T., Timmreck, C., Toohey, M., Tummon, F., Zanchettin, D., Zhu, Y., and Toon, O. B.: Model physics and chemistry causing intermodel disagreement within the VolMIP-Tambora Interactive Stratospheric Aerosol ensemble, Atmos. Chem. Phys., 21, 3317–3343, https://doi.org/10.5194/acp-21-3317-2021, 2021.

Coupe, J. and Robock, A.: The Influence of Stratospheric Soot and Sulfate Aerosols on the Northern Hemisphere Wintertime Atmospheric Circulation, J. Geophys. Res. Atmos., 126, https://doi.org/10.1029/2020jd034513, 2021.

Danabasoglu, G., Lamarque, J. Bacmeister, J., Bailey, D. A., DuVivier, A. K. , Edwards, J., Emmons, L. K., Fasullo, J., Garcia, R., Gettelman, A., Hannay, C., Holland, M. M., Large, W. G., Lauritzen, P. H., Lawrence, D. M., Lenaerts, J. T. M., Lindsay, K., Lipscomb, W. H., Mills, M. J., Neale, R., Oleson, K. W., Otto-Bliesner, B., Phillips, A. S., Sacks, W., Tilmes, S., Kampenhout, L., Vertenstein, M., Bertini, A., Dennis, J., Deser, C., Fischer, C., Fox-Kemper, B., Kay, J. E., Kinnison, D., Kushner, P. J., Larson, V. E., Long, M. C., Mickelson, S., Moore, J. K., Nienhouse, E., Polvani, L., Rasch, P. J., and Strand, W. G.: The Community Earth System Model Version 2 (CESM2), J. Adv. Model. Earth Syst., 12, https://doi.org/10.1029/2019ms001916, 2020.

Dhomse, S. S., Emmerson, K. M., Mann, G. W., Bellouin, N., Carslaw, K. S., Chipperfield, M. P., Hommel, R., Abraham, N. L., Telford, P., Braesicke, P., Dalvi, M., Johnson, C. E., O'Connor, F., Morgenstern, O., Pyle, J. A., Deshler, T., Zawodny, J. M., and Thomason, L. W.: Aerosol microphysics simulations of the Mt. Pinatubo eruption with the UM-UKCA composition-climate model, Atmos. Chem. Phys., 14, 11 221–11 246, https://doi.org/10.5194/acp-14-11221-2014, 2014.

Fuglestvedt, H., Zhuo, Z., Toohey, M., et al.: Revisiting the volcanic forcing of high-latitude Northern Hemisphere eruptions, https://doi.org/10.21203/rs.3.rs-3097917/v1, pREPRINT (Version 1) available at Research Square, 2023.

Gettelman, A., Mills, M. J., Kinnison, D. E., Garcia, R. R., Smith, A. K., Marsh, D. R., Tilmes, S., Vitt, F., Bardeen, C. G., McInerny, J., Liu, H. Solomon, S. C., Polvani, L. M., Emmons, L. K., Lamarque, J. Richter, J. H., Glanville, A. S., Bacmeister, J. T., Phillips, A. S.,

https://doi.org/10.5194/egusphere-2023-2374
Preprint. Discussion started: 1 December 2023

Neale, R. B., Simpson, I. R., DuVivier, A. K., Hodzic, A., and Randel, W. J.: The Whole Atmosphere Community Climate Model Version 6 (WACCM6), J. Geophys. Res. Atmos., 124, 12 380–12 403, https://doi.org/10.1029/2019jd030943, 2019.

Grant, W. B., Fishman, J., Browell, E. V., Brackett, V. G., Nganga, D., Minga, A., Cros, B., Veiga, R. E., Butler, C. F., Fenn, M. A., and Nowicki, G. D.: Observations of reduced ozone concentrations in the tropical stratosphere after the eruption of Mt. Pinatubo, Geophys. Res. Lett., 19, 1109–1112, https://doi.org/https://doi.org/10.1029/92GL01153, 1992.

Guo, S., Bluth, G. J. S., Rose, W. I., Watson, I. M., and Prata, A. J.: Re-evaluation of SO2release of the 15 June 1991 Pinatubo eruption using ultraviolet and infrared satellite sensors, Geochem. Geophys. Geosystems, 5, n/a–n/a, https://doi.org/10.1029/2003gc000654, 2004.

Hunke, E. C., Lipscomb, W. H., Turner, A. K., Jeffery, N., and Elliott, S.: CICE: The Los Alamos Sea Ice Model. Documentation and Software User's Manual. Version 5.1. T-3 Fluid Dynamics Group, Los Alamos National Laboratory, Report Tech. Rep. LA-CC-06-012, 2015.

IPCC: Climate Change 2013: The Physical Science Basis. Contribution of Working Group I to the Fifth Assessment Report of the Intergovernmental Panel on Climate Change, Cambridge University Press, Cambridge, United Kingdom and New York, NY, USA, 2013.

Jones, A. C., Haywood, J. M., Jones, A., and Aquila, V.: Sensitivity of volcanic aerosol dispersion to meteorological conditions: A Pinatubo case study, J. Geophys. Res. Atmos., 121, 6892–6908, https://doi.org/10.1002/2016jd025001, 2016.

Jungclaus, J. H., Bard, E., Baroni, M., Braconnot, P., Cao, J., Chini, L. P., Egorova, T., Evans, M., González-Rouco, J. F., Goosse, H., Hurtt, G. C., Joos, F., Kaplan, J. O., Khodri, M., Klein Goldewijk, K., Krivova, N., LeGrande, A. N., Lorenz, S. J., Luterbacher, J., Man, W., Maycock, A. C., Meinshausen, M., Moberg, A., Muscheler, R., Nehrbass-Ahles, C., Otto-Bliesner, B. I., Phipps, S. J., Pongratz, J., Rozanov, E., Schmidt, G. A., Schmidt, H., Schmutz, W., Schurer, A., Shapiro, A. I., Sigl, M., Smerdon, J. E., Solanki, S. K., Timmreck, C., Toohey, M., Usoskin, I. G., Wagner, S., Wu, C.-J., Yeo, K. L., Zanchettin, D., Zhang, Q., and Zorita, E.: The PMIP4 contribution to CMIP6 – Part 3: The last millennium, scientific objective, and experimental design for the PMIP4 lt;igt;past1000lt;/igt; simulations, Geosci. Model Dev., 10, 4005–4033, https://doi.org/10.5194/gmd-10-4005-2017, 2017.

Khodri, M., Izumo, T., Vialard, J., Janicot, S., Cassou, C., Lengaigne, M., Mignot, J., Gastineau, G., Guilyardi, E., Lebas, N., Robock, A., and McPhaden, M. J.: Tropical explosive volcanic eruptions can trigger El Nino by cooling tropical Africa, Nat. Commun., 8, 778, https://doi.org/10.1038/s41467-017-00755-6, 2017.

Klobas, E. J., Wilmouth, D. M., Weisenstein, D. K., Anderson, J. G., and Salawitch, R. J.: Ozone depletion following future volcanic eruptions, Geophys. Res. Lett., 44, 7490–7499, https://doi.org/10.1002/2017gl073972, 2017.

Krüger, K., Kutterolf, S., and Hansteen, T. H.: Halogen release from Plinian eruptions and depletion of stratospheric ozone, pp. 244–259, Cambridge University Press, Cambridge, https://doi.org/10.1017/CBO9781107415683.020, 2015.

Kutterolf, S., Hansteen, T. H., Appel, K., Freundt, A., Krüger, K., Pérez, W., and Wehrmann, H.: Combined bromine and chlorine release from large explosive volcanic eruptions: A threat to stratospheric ozone?, Geology, 41, 707–710, https://doi.org/10.1130/g34044.1, 2013.

Kutterolf, S., Hansteen, T. H., Freundt, A., Wehrmann, H., Appel, K., Krüger, K., and Pérez, W.: Bromine and chlorine emissions from Plinian eruptions along the Central American Volcanic Arc: From source to atmosphere, Earth Planet. Sci. Lett., 429, 234–246, https://doi.org/10.1016/j.epsl.2015.07.064, 2015.

Lacis, A.: Volcanic aerosol radiative properties, Past Global Changes Magazine, 23, 50–51, https://doi.org/10.22498/pages.23.2.50, 2015.

Lawrence, D. M., Fisher, R. A., Koven, C. D., Oleson, K. W., Swenson, S. C., Bonan, G., Collier, N., Ghimire, B., van Kampenhout, L., Kennedy, D., Kluzek, E., Lawrence, P. J., Li, F., Li, H., Lombardozzi, D., Riley, W. J., Sacks, W. J., Shi, M., Vertenstein, M., Wieder, W. R., Xu, C., Ali, A. A., Badger, A. M., Bisht, G., van den Broeke, M., Brunke, M. A., Burns, S. P., Buzan, J., Clark, M., Craig, A., Dahlin, K., Drewniak, B., Fisher, J. B., Flanner, M., Fox, A. M., Gentine, P., Hoffman, F., Keppel-Aleks, G., Knox, R., Kumar, S., Lenaerts, J., Leung,

https://doi.org/10.5194/egusphere-2023-2374
Preprint. Discussion started: 1 December 2023

L. R., Lipscomb, W. H., Lu, Y., Pandey, A., Pelletier, J. D., Perket, J., Randerson, J. T., Ricciuto, D. M., Sanderson, B. M., Slater, A., Subin, Z. M., Tang, J., Thomas, R. Q., Val Martin, M., and Zeng, X.: The Community Land Model Version 5: Description of New Features, Benchmarking, and Impact of Forcing Uncertainty, J. Adv. Model. Earth Syst., 11, 4245–4287, https://doi.org/10.1029/2018ms001583, 2019.

Lipscomb, W. H., Price, S. F., Hoffman, M. J., Leguy, G. R., Bennett, A. R., Bradley, S. L., Evans, K. J., Fyke, J. G., Kennedy, J. H., Perego, M., Ranken, D. M., Sacks, W. J., Salinger, A. G., Vargo, L. J., and Worley, P. H.: Description and evaluation of the Community Ice Sheet Model (CISM) v2.1, Geosci. Model Dev., 12, 387–424, https://doi.org/10.5194/gmd-12-387-2019, 2019.

Liu, X., Easter, R. C., Ghan, S. J., Zaveri, R., Rasch, P., Shi, X., Lamarque, J. F., Gettelman, A., Morrison, H., Vitt, F., Conley, A., Park, S., Neale, R., Hannay, C., Ekman, A. M. L., Hess, P., Mahowald, N., Collins, W., Iacono, M. J., Bretherton, C. S., Flanner, M. G., and Mitchell, D.: Toward a minimal representation of aerosols in climate models: description and evaluation in the Community Atmosphere Model CAM5, Geosci. Model Dev., 5, 709–739, https://doi.org/10.5194/gmd-5-709-2012, 2012.

Liu, X., Ma, P. L., Wang, H., Tilmes, S., Singh, B., Easter, R. C., Ghan, S. J., and Rasch, P. J.: Description and evaluation of a new four-mode version of the Modal Aerosol Module (MAM4) within version 5.3 of the Community Atmosphere Model, Geosci. Model Dev., 9, 505–522, https://doi.org/10.5194/gmd-9-505-2016, 2016.

Lurton, T., Jégou, F., Berthet, G., Renard, J.-B., Clarisse, L., Schmidt, A., Brogniez, C., and Roberts, T. J.: Model simulations of the chemical and aerosol microphysical evolution of the Sarychev Peak 2009 eruption cloud compared to in situ and satellite observations, Atmos. Chem. Phys., 18, 3223–3247, https://doi.org/10.5194/acp-18-3223-2018, 2018.

Marshall, L., Schmidt, A., Toohey, M., Carslaw, K. S., Mann, G. W., Sigl, M., Khodri, M., Timmreck, C., Zanchettin, D., Ball, W. T., Bekki, S., Brooke, J. S. A., Dhomse, S., Johnson, C., Lamarque, J.-F., LeGrande, A. N., Mills, M. J., Niemeier, U., Pope, J. O., Poulain, V., Robock, A., Rozanov, E., Stenke, A., Sukhodolov, T., Tilmes, S., Tsigaridis, K., and Tummon, F.: Multi-model comparison of the volcanic sulfate deposition from the 1815 eruption of Mt. Tambora, Atmos. Chem. Phys., 18, 2307–2328, https://doi.org/10.5194/acp-18-2307-2018, 2018.

Marshall, L., Johnson, J. S., Mann, G. W., Lee, L., Dhomse, S. S., Regayre, L., Yoshioka, M., Carslaw, K. S., and Schmidt, A.: Exploring How Eruption Source Parameters Affect Volcanic Radiative Forcing Using Statistical Emulation, J. Geophys. Res. Atmos., 124, 964–985, https://doi.org/10.1029/2018jd028675, 2019.

Metzner, D., Kutterolf, S., Toohey, M., Timmreck, C., Niemeier, U., Freundt, A., and Krüger, K.: Radiative forcing and climate impact resulting from SO2 injections based on a 200,000-year record of Plinian eruptions along the Central American Volcanic Arc, Int. J. Earth Sci., 103, 2063–2079, https://doi.org/10.1007/s00531-012-0814-z, 2014.

Mills, M. J., Schmidt, A., Easter, R., Solomon, S., Kinnison, D. E., Ghan, S. J., Neely, R. R., Marsh, D. R., Conley, A., Bardeen, C. G., and Gettelman, A.: Global volcanic aerosol properties derived from emissions, 1990–2014, using CESM1(WACCM), J. Geophys. Res. Atmos., 121, 2332–2348, https://doi.org/10.1002/2015jd024290, 2016.

Mills, M. J., Richter, J. H., Tilmes, S., Kravitz, B., MacMartin, D. G., Glanville, A. A., Tribbia, J. J., Vitt, J.-F. L. F., Schmidt, A., Gettelman, A., Hannay, C., Bacmeister, J. T., and Kinnison, D. E.: Radiative and chemical response to interactive stratospheric sulfate aerosols in fully coupled CESM1(WACCM), J. Geophys. Res. Atmos., 122, 13,061–13,078, https://doi.org/10.1002/ 2017JD027006, 2017.

Ming, A., Winton, V. H. L., Keeble, J., Abraham, N. L., Dalvi, M. C., Griffiths, P., Caillon, N., Jones, A. E., Mulvaney, R., Savarino, J., Frey, M. M., and Yang, X.: Stratospheric Ozone Changes From Explosive Tropical Volcanoes: Modeling and Ice Core Constraints, J. Geophys. Res. Atmos., 125, https://doi.org/10.1029/2019jd032290, 2020.

https://doi.org/10.5194/egusphere-2023-2374
Preprint. Discussion started: 1 December 2023

Neu, J. L. and Plumb, R. A.: Age of air in a "leaky pipe" model of stratospheric transport, J. Geophys. Res. Atmos., 104, 19 243–19 255, https://doi.org/10.1029/1999jd900251, 1999.

Niemeier, U., Timmreck, C., Graf, H.-F., Kinne, S., Rast, S., and Self, S.: Initial fate of fine ash and sulfur from large volcanic eruptions, Atmos. Chem. Phys., 9, 9043–9057, https://doi.org/www.atmos-chem-phys.net/9/9043/2009/, 2009.

Pausata, F. S. R., Karamperidou, C., Caballero, R., and Battisti, D. S.: ENSO response to high-latitude volcanic eruptions in the Northern Hemisphere: The role of the initial conditions, Geophys. Res. Lett., 43, 8694–8702, https://doi.org/https://doi.org/10.1002/2016GL069575, 2016.

Pausata, F. S. R., Zanchettin, D., Karamperidou, C., Caballero, R., and Battisti, D. S.: ITCZ shift and extratropical teleconnections drive ENSO response to volcanic eruptions, Sci. Adv., 6, eaaz5006, https://doi.org/doi:10.1126/sciadv.aaz5006, 2020.

Quaglia, I., Timmreck, C., Niemeier, U., Visioni, D., Pitari, G., Brodowsky, C., Brühl, C., Dhomse, S. S., Franke, H., Laakso, A., Mann, G. W., Rozanov, E., and Sukhodolov, T.: Interactive stratospheric aerosol models' response to different amounts and altitudes of SO2 injection during the 1991 Pinatubo eruption, Atmos. Chem. Phys., 23, 921–948, https://doi.org/10.5194/acp-23-921-2023, 2023.

Ribera, P., Peña-Ortiz, C., Garcia-Herrera, R., Gallego, D., Gimeno, L., and Hernández, E.: Detection of the secondary meridional circulation associated with the quasi-biennial oscillation, J. Geophys. Res., 109, https://doi.org/10.1029/2003jd004363, 2004.

Robock, A.: Volcanic eruptions and climate, Rev. Geophys., 38, 191–219, https://doi.org/10.1029/1998rg000054, 2000.

Schneider, D. P., Ammann, C. M., Otto-Bliesner, B. L., and Kaufman, D. S.: Climate response to large, high-latitude and low-latitude volcanic eruptions in the Community Climate System Model, J. Geophys. Res., 114, https://doi.org/10.1029/2008jd011222, 2009.

Sigl, M., Winstrup, M., McConnell, J. R., Welten, K. C., Plunkett, G., Ludlow, F., Buntgen, U., Caffee, M., Chellman, N., Dahl-Jensen, D., Fischer, H., Kipfstuhl, S., Kostick, C., Maselli, O. J., Mekhaldi, F., Mulvaney, R., Muscheler, R., Pasteris, D. R., Pilcher, J. R., Salzer, M., Schupbach, S., Steffensen, J. P., Vinther, B. M., and Woodruff, T. E.: Timing and climate forcing of volcanic eruptions for the past 2,500 years, Nature, 523, 543–9, https://doi.org/10.1038/nature14565, 2015.

Sigl, M., Toohey, M., McConnell, J. R., Cole-Dai, J., and Severi, M.: Volcanic stratospheric sulfur injections and aerosol optical depth during the Holocene (past 11 500 years) from a bipolar ice-core array, Earth Syst. Sci. Data, 14, 3167–3196, https://doi.org/10.5194/essd-14-3167-2022, 2022.

Smith, R., Jones, P., Briegleb, B., Bryan, F., Danabasoglu, G., Dennis, J., et al.: The Parallel Ocean Program (POP) reference manual, Ocean component of the Community Climate System Model (CCSM), Tech. Rep. LAUR-10-01853, LANL Tech. Report, 2010.

Solomon, S.: Stratospheric ozone depletion: A review of concepts and history, Rev. Geophys., 37, 275–316, https://doi.org/10.1029/1999rg900008, 1999.

Staunton-Sykes, J., Aubry, T. J., Shin, Y. M., Weber, J., Marshall, L. R., Luke Abraham, N., Archibald, A., and Schmidt, A.: Co-emission of volcanic sulfur and halogens amplifies volcanic effective radiative forcing, Atmos. Chem. Phys., 21, 9009–9029, https://doi.org/10.5194/acp-21-9009-2021, 2021.

Stenchikov, G., Ukhov, A., Osipov, S., Ahmadov, R., Grell, G., Cady-Pereira, K., Mlawer, E., and Iacono, M.: How Does a Pinatubo-Size Volcanic Cloud Reach the Middle Stratosphere?, J. Geophys. Res. Atmos., 126, https://doi.org/10.1029/2020jd033829, 2021.

Stier, P., Feichter, J., Kinne, S., Kloster, S., Vignati, E., Wilson, J., Ganzeveld, L., Tegen, I., Werner, M., Balkanski, Y., Schulz, M., Boucher, O., Minikin, A., and Petzold, A.: The aerosol-climate model ECHAM5-HAM, Atmos. Chem. Phys., 5, 1125–1156, https://doi.org/10.5194/acp-5-1125-2005, 2005.

Timmreck, C.: Modeling the climatic effects of large explosive volcanic eruptions, Wiley Interdiscip. Rev. Clim. Change, 3, 545–564, https://doi.org/10.1002/wcc.192, 2012.

https://doi.org/10.5194/egusphere-2023-2374
Preprint. Discussion started: 1 December 2023

Timmreck, C., Mann, G. W., Aquila, V., Hommel, R., Lee, L. A., Schmidt, A., Brühl, C., Carn, S., Chin, M., Dhomse, S. S., Diehl, T., English, J. M., Mills, M. J., Neely, R., Sheng, J., Toohey, M., and Weisenstein, D.: The Interactive Stratospheric Aerosol Model Intercomparison Project (ISA-MIP): motivation and experimental design, Geosci. Model Dev., 11, 2581–2608, https://doi.org/10.5194/gmd-11-2581-2018, 2018.

Toohey, M. and Sigl, M.: Volcanic stratospheric sulfur injections and aerosol optical depth from 500BCE to 1900CE, Earth Syst. Sci. Data, 9, 809–831, https://doi.org/10.5194/essd-9-809-2017, 2017.

Toohey, M., Krüger, K., Niemeier, U., and Timmreck, C.: The influence of eruption season on the global aerosol evolution and radiative impact of tropical volcanic eruptions, Atmos. Chem. Phys., 11, 12 351–12 367, https://doi.org/10.5194/acp-11-12351-2011, 2011.

Toohey, M., Krüger, K., Bittner, M., Timmreck, C., and Schmidt, H.: The impact of volcanic aerosol on the Northern Hemisphere stratospheric polar vortex: mechanisms and sensitivity to forcing structure, Atmos. Chem. Phys., 14, 13 063–13 079, https://doi.org/10.5194/acp-14-13063-2014, 2014.

Toohey, M., Stevens, B., Schmidt, H., and Timmreck, C.: Easy Volcanic Aerosol (EVA v1.0): an idealized forcing generator for climate simulations, Geosci. Model Dev., 9, 4049–4070, https://doi.org/10.5194/gmd-9-4049-2016, 2016.

Toohey, M., Krüger, K., Schmidt, H., Timmreck, C., Sigl, M., Stoffel, M., and Wilson, R.: Disproportionately strong climate forcing from extratropical explosive volcanic eruptions, Nat. Geosci., 12, 100–107, https://doi.org/10.1038/s41561-018-0286-2, 2019.

Ukhov, A., Stenchikov, G., Osipov, S., Krotkov, N., Gorkavyi, N., Li, C., Dubovik, O., and Lopatin, A.: Inverse Modeling of the Initial Stage of the 1991 Pinatubo Volcanic Cloud Accounting for Radiative Feedback of Volcanic Ash, J. Geophys. Res. Atmos., 128, e2022JD038 446, https://doi.org/https://doi.org/10.1029/2022JD038446, e2022JD038446 2022JD038446, 2023.

van Loon, H. and Labitzke, K.: The Southern Oscillation. Part V: The Anomalies in the Lower Stratosphere of the Northern Hemisphere in Winter and a Comparison with the Quasi-Biennial Oscillation, Monthly Weather Review, 115, 357–369, https://doi.org/10.1175/1520-0493(1987)115<0357:Tsopvt>2.0.Co;2, 1987.

von Glasow, R., Bobrowski, N., and Kern, C.: The effects of volcanic eruptions on atmospheric chemistry, Chem. Geol., 263, 131–142, https://doi.org/10.1016/j.chemgeo.2008.08.020, 2009.

WMO: Scientific Assessment of Ozone Depletion: 2018, Global Ozone Research and Monitoring Project, Report No. 58, csl.noaa.gov/assessments/ozone/2018/downloads/2018OzoneAssessment.pdf, 2018.

Zanchettin, D., Khodri, M., Timmreck, C., Toohey, M., Schmidt, A., Gerber, E. P., Hegerl, G., Robock, A., Pausata, F. S. R., Ball, W. T., Bauer, S. E., Bekki, S., Dhomse, S. S., LeGrande, A. N., Mann, G. W., Marshall, L., Mills, M., Marchand, M., Niemeier, U., Poulain, V., Rozanov, E., Rubino, A., Stenke, A., Tsigaridis, K., and Tummon, F.: The Model Intercomparison Project on the climatic response to Volcanic forcing (VolMIP): experimental design and forcing input data for CMIP6, Geosci. Model Dev., 9, 2701–2719, https://doi.org/10.5194/gmd-9-2701-2016, 2016.

Zanchettin, D., Timmreck, C., Khodri, M., Schmidt, A., Toohey, M., Abe, M., Bekki, S., Cole, J., Fang, S.-W., Feng, W., Hegerl, G., Johnson, B., Lebas, N., LeGrande, A. N., Mann, G. W., Marshall, L., Rieger, L., Robock, A., Rubinetti, S., Tsigaridis, K., and Weierbach, H.: Effects of forcing differences and initial conditions on inter-model agreement in the VolMIP volc-pinatubo-full experiment, Geosci. Model Dev., 15, 2265–2292, https://doi.org/10.5194/gmd-15-2265-2022, 2022.

Zhu, Y., Toon, O. B., Jensen, E. J., Bardeen, C. G., Mills, M. J., Tolbert, M. A., Yu, P., and Woods, S.: Persisting volcanic ash particles impact stratospheric SO2 lifetime and aerosol optical properties, Nat. Commun., 11, 4526, https://doi.org/10.1038/s41467-020-18352-5, 2020.

Zhuo, Z., Gao, C., and Pan, Y.: Proxy evidence for China's monsoon precipitation response to volcanic aerosols over the past seven centuries, J. Geophys. Res. Atmos., 119, 6638–6652, https://doi.org/https://doi.org/10.1002/2013JD021061, 2014.

https://doi.org/10.5194/egusphere-2023-2374
Preprint. Discussion started: 1 December 2023

Zhuo, Z., Kirchner, I., Pfahl, S., and Cubasch, U.: Climate impact of volcanic eruptions: the sensitivity to eruption season and latitude in MPI-ESM ensemble experiments, Atmos. Chem. Phys., 21, 13 425–13 442, https://doi.org/10.5194/acp-21-13425-2021, 2021.

https://doi.org/10.5194/egusphere-2023-2374
Preprint. Discussion started: 1 December 2023

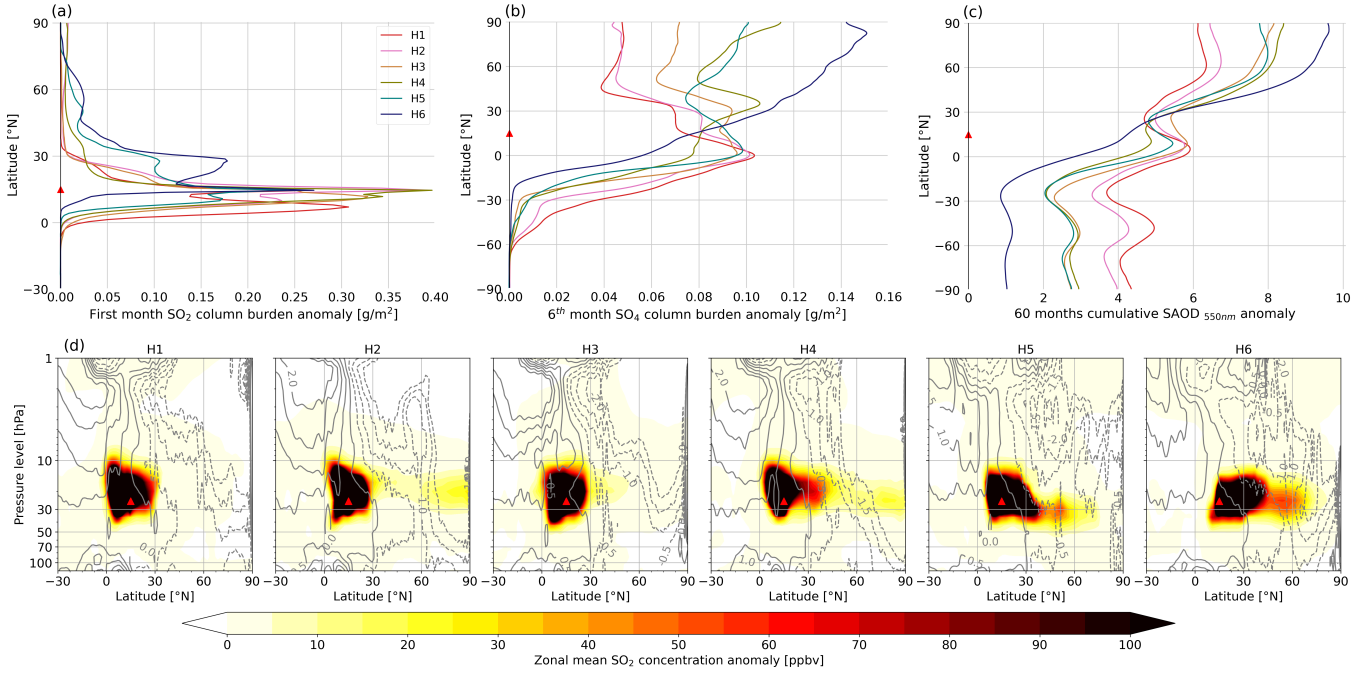

Figure 1. Latitudinal distribution of the first month SO_2 column burden anomaly (a), the sixth month SO_4 column burden anomaly (b), 60 months cumulative SAOD anomaly at 550 nm (c), and the first month latitudinal and vertical distribution of SO_2 concentration anomaly (shades), and residual vertical velocity (w*, contours with an interval of 0.5 mm s^{-1}) (d) in the stratosphere after tropical eruptions in January for six members of the baseline experiments. The ensemble members are ordered in an ascending trend of northward SO_2 transport in the first month. The red triangle indicates the eruption latitude at 15° N in (a-c), and also the injection altitude at 24 km in (d).

https://doi.org/10.5194/egusphere-2023-2374
Preprint. Discussion started: 1 December 2023

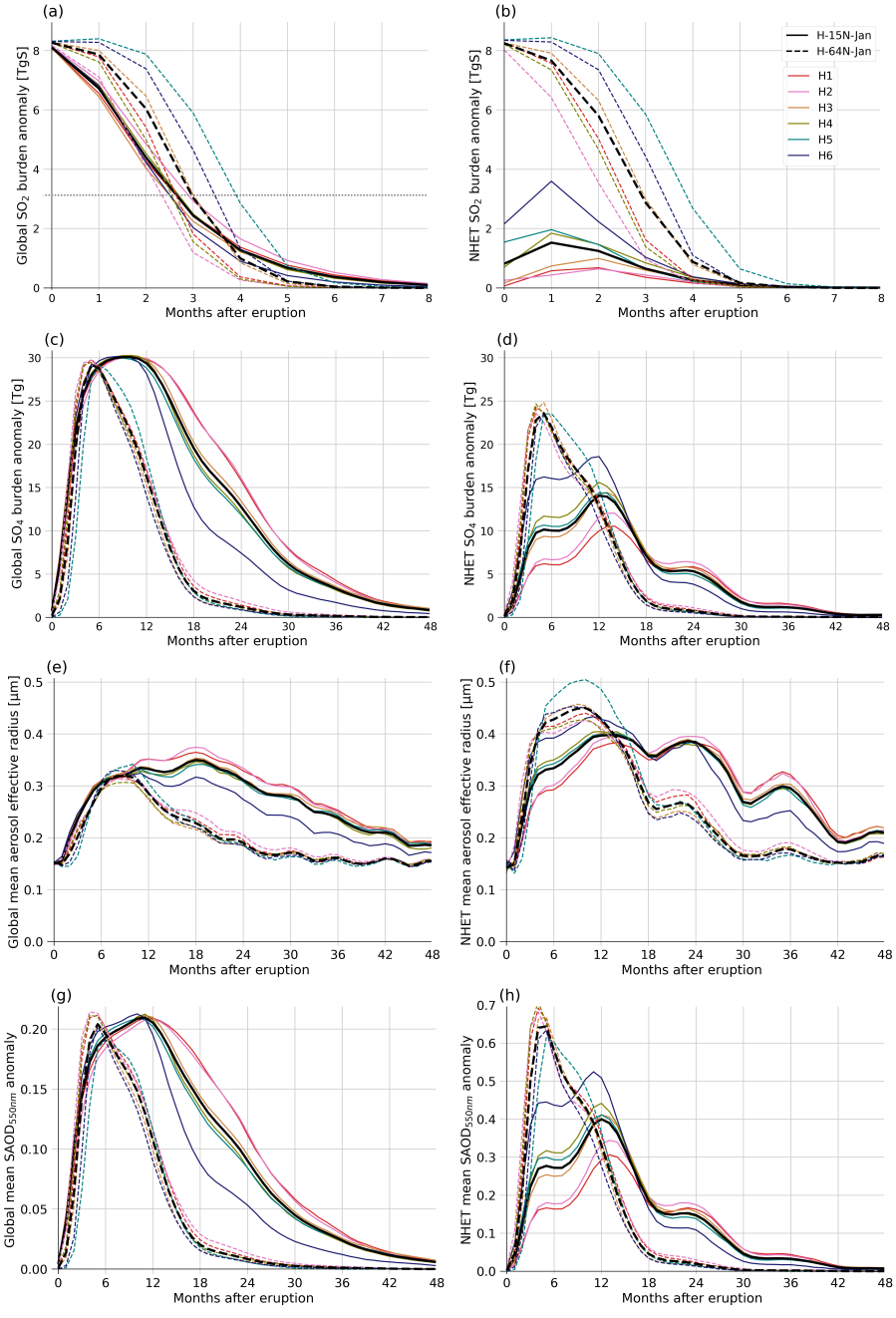

Figure 2. Global (left panel) and Northern Hemisphere extratropics (NHET, right panel) SO_2 (a, b), SO_4 (c, d) burden anomaly, aerosol effective radius (R_{eff}, e, f) and stratospheric aerosol optical depth (SAOD, g, h). Solid lines and dashed lines are for tropical and NH extratropical eruptions, respectively. Different colors represent different ensemble member realizations. The black lines represent the ensemble means of the baseline experiments. The gray dotted horizontal line in (a) represents the e–folding of injected sulfur. Note the different axes in different subfigures.

https://doi.org/10.5194/egusphere-2023-2374
Preprint. Discussion started: 1 December 2023

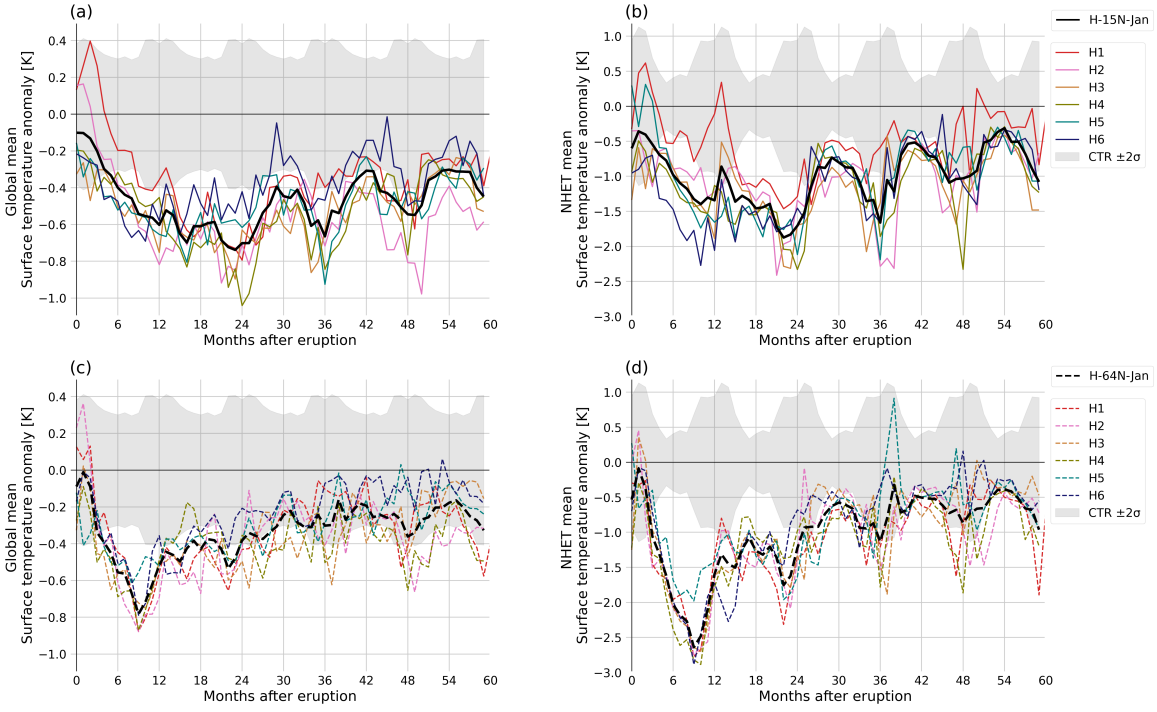

Figure 3. Global (left panel) and Northern Hemisphere extratropics (NHET, right panel) mean surface temperature anomaly. Solid lines and dashed lines are for tropical (a–b) and NH extratropical (c–d) eruptions, respectively. Different colors represent different ensemble member realizations. The black lines represent the ensemble means of the baseline experiments. The gray shades represent two standard deviations of the control run. Note the different y–axes between the left and right panels.

https://doi.org/10.5194/egusphere-2023-2374
Preprint. Discussion started: 1 December 2023

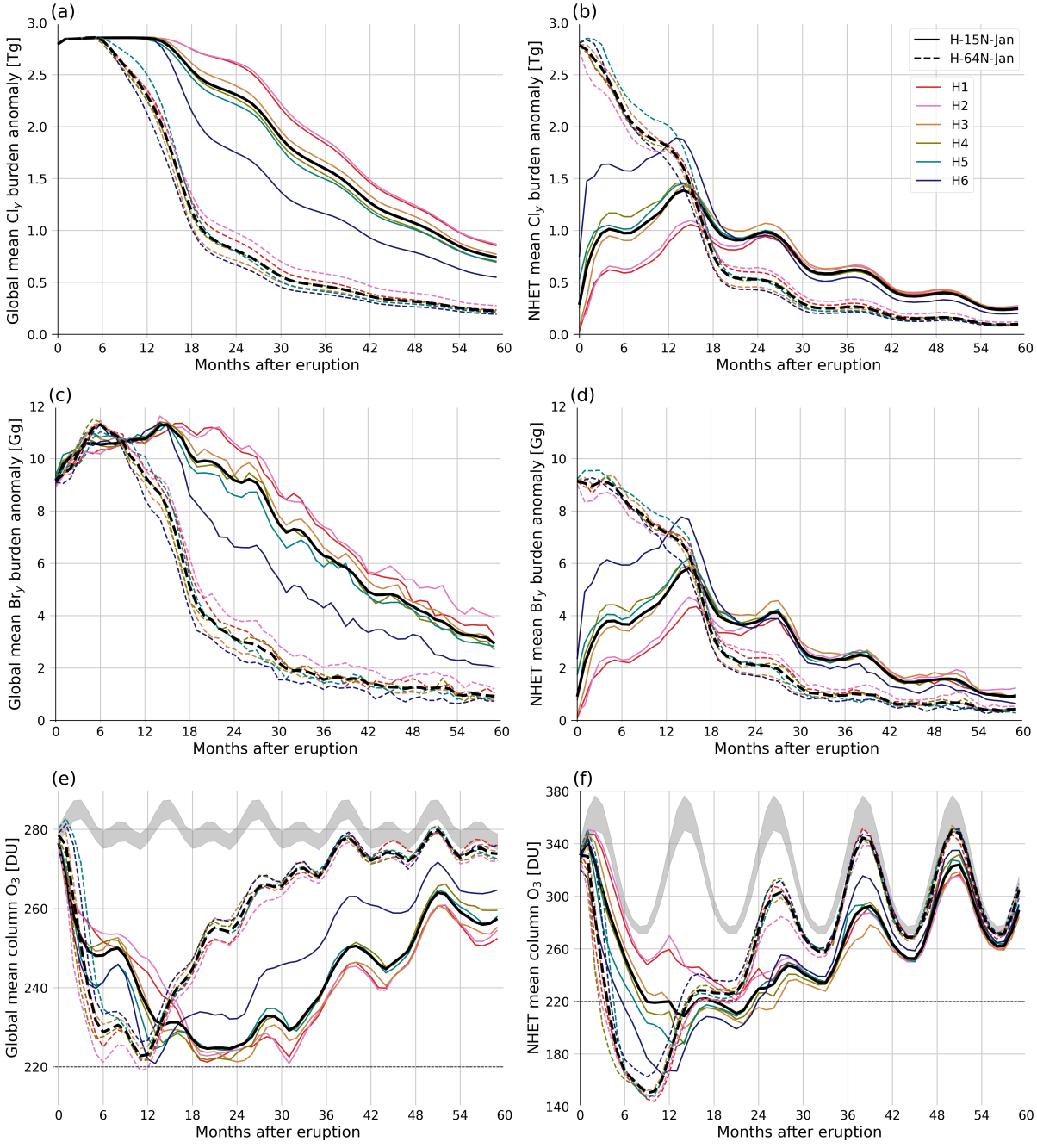

Figure 4. Global (left panel) and Northern Hemisphere extratropics (NHET, right panel) total inorganic Chlorine (Cl_y = Cl + ClO + $2Cl_2$ + $2Cl_2O_2$ + OClO + HOCl + $ClONO_2$ + HCl+ BrCl, a, b) and total inorganic bromine (Br_y = Br + BrO + HOBr + $BrONO_2$ + HBr + BrCl, c, d) burden anomaly and global and NHET mean column O_3 (e, f). Solid lines are variations after tropical eruptions, while dashed lines are variations after NH extratropical eruptions. Different colors represent different ensemble member realizations. The black lines represent the ensemble means of the baseline experiments. The gray dotted horizontal line in (a) and (c) represents the e-folding of injected halogens. The gray shades (e, f) represent two standard deviations of the control run.

https://doi.org/10.5194/egusphere-2023-2374
Preprint. Discussion started: 1 December 2023

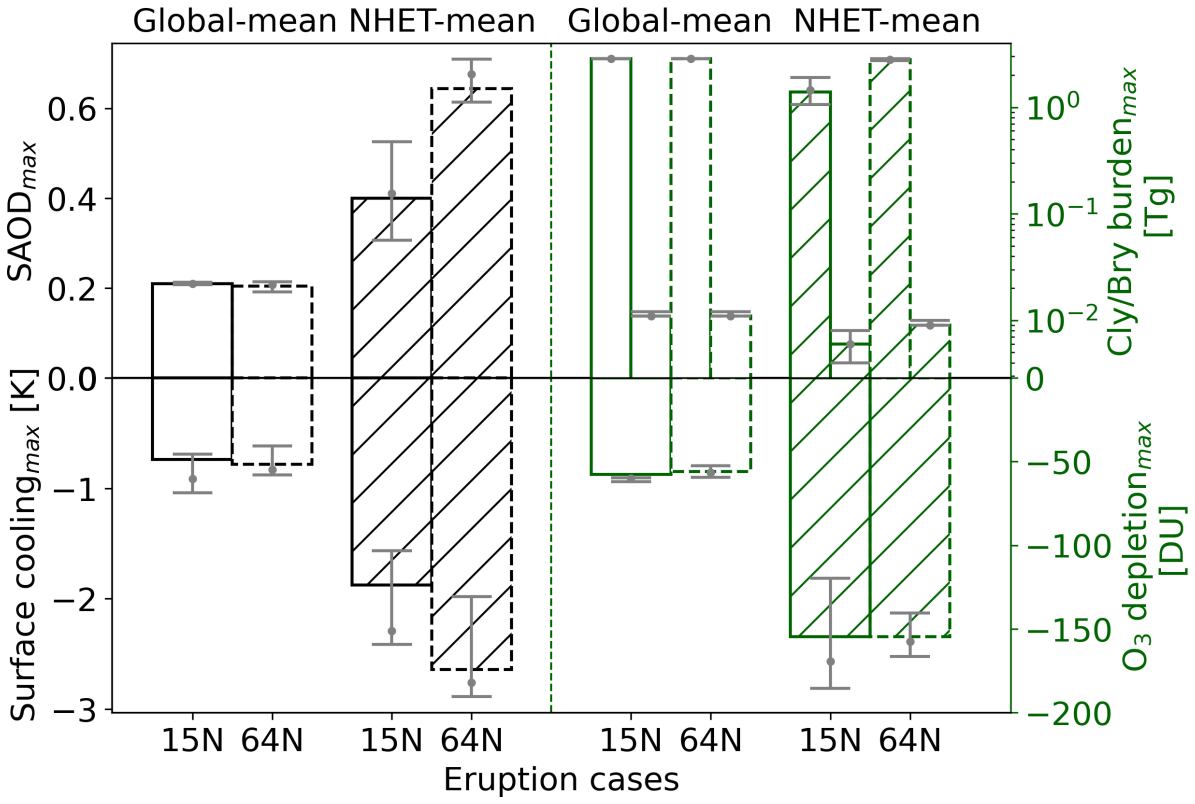

Figure 5. Summary of global–mean and NHET–mean maximum volcanic forcing (left top part), surface cooling (left bottom part), halogen burden (right top part) and ozone depletion (right bottom part) between tropical and NH extratropical volcanic eruptions at 15° N (solid bars) and 64° N (dashed bars), respectively. The grey error bars and grey dots indicate the range and median of the six ensemble members of the baseline experiments.

https://doi.org/10.5194/egusphere-2023-2374
Preprint. Discussion started: 1 December 2023

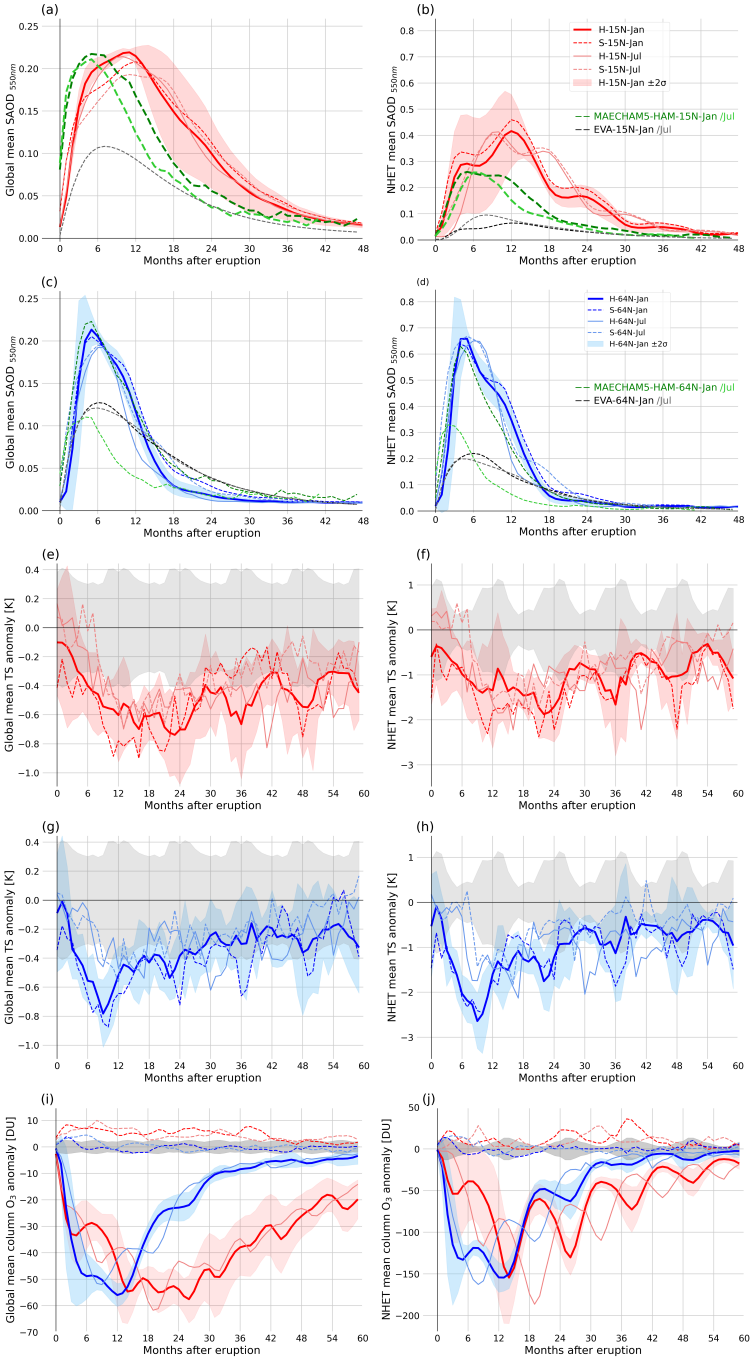

Figure 6. Global (left panel) and Northern Hemisphere extratropics (NHET, right panel) mean stratospheric aerosol optical depth (SAOD) at 550 nm (a–d), surface temperature anomaly (e–h) and column ozone anomaly (i, j) after tropical and NH extratropical eruptions. The shades represent two standard deviations of the baseline ensemble experiments. Red and blue color lines and shades represent variations after tropical and NH extratropical eruptions, respectively. The solid and dashed lines are simulated volcanic eruptions with co–injection of sulfur and halogen and sulfur–only injection, respectively. The gray shades (e–j) represent two standard deviations of the control run. Note the different y–axes between the left and right panels.

https://doi.org/10.5194/egusphere-2023-2374
Preprint. Discussion started: 1 December 2023

Table 1. Summary of model experiments with CESM2–WACCM6. In addition, MAECHAM5–HAM (ECHAM5) and EVA as stated.

Tropical eruptions CAVA *: 15° N, 91° W	Extratropical eruptions Iceland: 64° N, 19° W	Ensemble member	QBO @ 30 hPa	ENSO (ONI)	Polar Vortex †	Injection @ 24km altitude SO_2 [Tg]	HCl* [Tg]	HBr * [Gg]
H–15N–Jan #	H–64N–Jan #	H1	Westerly	El Niño	3	17	2.93	9.5
		H2	Westerly	El Niño	1			
		H3	Westerly	Neutral	4			
		H4	Westerly	Neutral	2			
		H5	Westerly	La Niña	6			
		H6	Westerly	La Niña	5			
S–15N–Jan	S–64N–Jan	—	Westerly	neutral	4	17	—	—
H–15N–Jul	H–64N–Jul	—	Westerly	neutral	—	17	2.93	9.5
S–15N–Jul	S–64N–Jul	—	Westerly	neutral	—	17	—	—
ECHAM5–15N–Jan #	ECHAM5–64N–Jan	—	—	—	—	17	—	—
ECHAM5–15N–Jul #	ECHAM5–64N–Jul	—	—	—	—	17	—	—
EVA–15N–Jan	EVA–64N–Jan	—	—	—	—	17	—	—
EVA–15N–Jul	EVA–64N–Jul	—	—	—	—	17	—	—

* HCl and HBr masses were scaled based on petrological measurements from Central American Volcanic Arc (CAVA) volcanoes (Kutterolf et al., 2015, 2013), assuming a 10% injection efficiency to the stratosphere (Krüger et al., 2015; Brenna et al., 2019).

†Numbers of initial polar vortex (PV) states as in Fuglestvedt et al. (2023).

Ensemble mean.